Wheat endosperm as a cohesive granular material

Vincent Topin[a,b,*], Farhang Radjaï[a], Jean-Yves Delenne[a], Abdelkrim Sadoudi[b], Frédéric Mabille[b]

[a]*LMGC, CNRS-Université Montpellier II, Place Eugène Bataillon, 34095 Montpellier cedex 5, France*
[b]*IATE, CNRS-INRA, 2 place Pierre Viala, 34060 Montpellier cedex 1, France*

We introduce a cohesive granular model of the wheat endosperm involving a discrete phase composed of starch granules, a continuous phase representing the protein matrix and pores. The cohesion of the texture is governed by adherence between starch and protein, reflecting the biochemical nature of the interface, and the protein content that controls the connectivity between starch granules. We present a detailed parametric study of the stiffness, yield strength and regimes of crack propagation under tensile loading. We then show that starch damage, as a descriptor of wheat hardness, scales with the relative toughness between the starch and the starch–protein interface. The toughness appears therefore to be the control parameter governing transition from 'soft' to 'hard' behavior. Interestingly, this parameter combines the starch–protein adherence with protein content, two major quantities often assumed to underly wheat hardness.

Keywords: Wheat endosperm; Lattice model; Cohesive granular media; Hardness; Fracture

1. Introduction

Wheat hardness variation is an important trait in the determination of end-use quality of wheat flours for food industry. Common classifications differentiate 'soft' and 'hard' (*T. aestivum*) wheat from 'very hard' or durum wheat (*T. durum*). Soft wheat kernels require less energy to mill and produce flour consisting of small aggregates of starch granules and protein, and many free starch granules. Hard wheat kernels grind to coarser aggregates and include damaged starch granules. Durum wheat kernels are very hard in texture and high in protein content (Turnbull and Rahman, 2002; Morris, 2002).

Three methods are generally used to determine wheat hardness: near-infrared reflectance (NIR), particle size index (PSI) and single-kernel characterization system (SKCS) (Morris, 2002). In contrast to SKCS, where the crushing strength of single grains are measured, in NIR and PSI methods the wheat grain hardness correspond rather to an empirical description of the particle size distribution (PSD) after milling than an *ab initio* mechanical property of the grain (Atwell, 2001; Dobraszczyk, 1994; Turnbull and Rahman, 2002).

It is generally assumed that the hardness is a consequence of adherence between starch and protein as a major biochemical characteristic of the endosperm (Barlow et al., 1973; Greenwell and Schofield, 1986; Glenn and Johnston, 1992; Turnbull and Rahman, 2002; Piot et al., 2000). In fact, micropenetrometer hardness tests indicate that the proper mechanical strengths of starch granules and the protein phase do not vary widely with wheat species (Barlow et al., 1973; Glenn and Johnston, 1992), implying that the nature of starch–protein interface differs between 'hard' and 'soft' varieties. In the case of 'hard' and 'very hard' wheat, interactions between starch and protein are strong contrary to 'soft' wheat in which the interactions are weaker (Atwell, 2001).

Although genetically, 'soft', 'hard' and 'durum' wheat grains are *qualitative* classes depending on the presence and nature of puroindoline proteins (Greenwell and Schofield,

*Corresponding author. LMGC, CNRS-Université Montpellier II, Place Eugène Bataillon, 34095 Montpellier cedex 5, France.
E-mail address: topin@lmgc.univ-montp2.fr (V. Topin).

1986; Morris, 2002), the hardness, as measured from the PSD of meals, is also an increasing function of the protein content determined by growing conditions and reflected in the grain vitreousness (Haddad et al., 2001; Morris, 2002; Turnbull and Rahman, 2002). In fact, vitreous kernels generally show higher strength in compression, higher density and larger protein content. However, no simple correlation can be established between vitreosity and grain hardness: vitreous and mealy kernels may be produced from 'soft', 'hard' and 'durum' wheats.

Hence, the precise roles played by starch–protein adherence, protein content and possibly other structural features of the endosperm texture need to be quantified. From mechanical viewpoint, a central issue is whether the hardness defined via grain processing is controlled by a unique strength property of the endosperm, e.g. the strength at crushing or the stiffness (Dobraszczyk, 1994).

In this paper, we propose a lattice model capable of representing the multi-phase structure of the wheat endosperm at the scale of starch granules and allowing for the computation of its elastic deformation, damage and fracture. Each phase and its boundaries are represented by lattice elements sharing the same properties and belonging to the same portion of space. A sample of the wheat endosperm is composed of starch granules, a continuous phase representing the protein matrix, and pores. This model provides a suitable framework in which the influence of various structural and material parameters of the wheat endosperm can be characterized. In particular, we are interested in the stiffness, mechanical strength and particle damage as a function of the protein volume fraction and starch–protein adherence.

In the following, we first describe the model and the numerical procedures which were used to generate numerical samples of wheat endosperm. Then, we present a parametric study where various mechanical properties are analyzed as a function of the protein content and starch–protein adherence. Finally, we show that our data are consistent with an interesting interpretation of the wheat hardness in terms of a single parameter combining the protein content and starch–protein adherence. We conclude with a summary of salient results and possible perspectives of this work. The details of the lattice model are given in the Appendix.

2. Numerical method

The endosperm texture varies depending on the variety and growing conditions. Starch granules occur in volume fractions ranging from 63% to 72% of the endosperm (Atwell, 2001). There are mainly two size populations of granules. The smaller nearly spherical granules (type B) are 2–10 μm in diameter and 80–85% of the total number of granules, whereas the large granules (type A) are lens-shaped and 20–25 μm in diameter. The protein matrix, varying from 6% to 20% in volume fraction, surrounds the granules (Pomeranz, 1988). Fig. 1(a) displays a scanning electron micrograph of the fracture surface of a hard endosperm. Both types of starch granules and the protein phase, visible mostly in the form of cavities left by dislodged granules, can be observed.

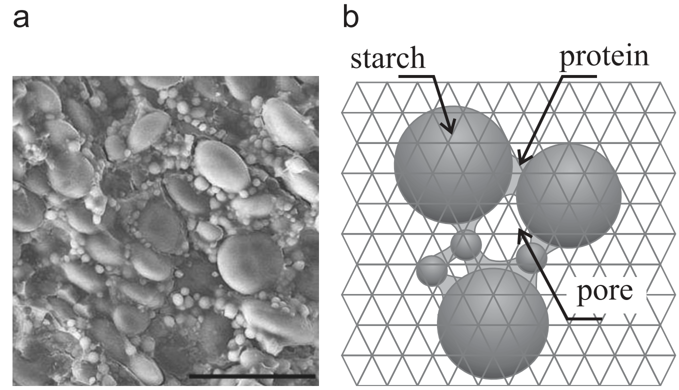

Fig. 1. (a) Scanning electron micrograph of the fracture surface of a hard endosperm (Falcon wheat) with scale bar equal to 50 μm; (b) representation of starch granules and the protein matrix on a triangular lattice.

The endosperm can be modeled as a granular solid composed of particles (starch granules) bound to one another by a cementing phase (corresponding to the protein matrix). In this picture, the scale-up of microscopic interactions to macroscopic properties is mediated by the granular nature of the endosperm. There are several discrete element methods for the simulation of granular media (Cundall and Strack, 1979; Moreau, 1994; Delenne, 2002; Radjaï et al., 2000–2001). In all these methods, the particles are assumed to be rigid and interacting via a contact law accounting for elastic repulsion, friction and cohesion. These methods cannot be used as such for the wheat endosperm since we would like to account also for the continuous matrix representing the protein phase. We need thus an intermediate approach between discrete element methods and the finite element method more commonly employed in materials science and structural engineering for the simulation of continuous media. This approach should also account for breakable interface elements (as interparticle contacts in granular media) and breakable bulk elements (as a damageable volume element in continua).

We rely on a lattice-type model which is a suitable framework for the simulation of heterogeneous materials (Roux, 1990; Schlangen and Garboczi, 1997; Van Mier et al., 1997). The three phases composing the wheat endosperm are thus discretized on the same lattice, the behavior and breaking characteristics of each phase being carried by lattice bonds. Different types of material behavior can be obtained for each phase in this way by incorporating elasto-plastic damageable bonds. When only strength parameters are of interest, simple elastic–brittle bonds can be used and large systems involving several hundred starch granules with a variable volume fraction of the protein can be simulated.

Lattice-type discretization has been used for statistical mechanics of fracture in disordered media, and applied to study the fracture properties of concrete, ceramics and soils (Cheng et al., 2002a,b; Chiaia et al., 1997; Delaplace et al., 1996; Feng et al., 1985; Herrmann and Roux, 1990; Gao and Klein, 1998; Lilliu and Van Mier, 2003; Prado and van Mier, 2003; Schlangen and Garboczi, 1997; Van Mier et al., 1997, 2002; Van Mier and Van Vliet, 1999; Vogel et al., 2005a,b). The space is discretized as a regular or disordered grid of nodes interconnected by one-dimensional elements or bonds. We use linear elastic–brittle elements defining a triangular lattice with an equilibrium element length. Each element is characterized by a Hooke constant and a breaking force threshold. Each phase and its frontiers are materialized by lattice bonds sharing the same properties and belonging to the same portion of space, see Fig. 1(b).

A sample is defined by its contour and the configuration of the phases in space. The samples are deformed by imposing displacements or forces to the nodes belonging to the contour. The initial state is the reference (unstressed) configuration. The total elastic energy of the system is a convex function of node displacements and thus finding the unique equilibrium configuration of the nodes amounts to a minimization problem. Performing this minimization for stepwise loading corresponds to subjecting the system to a quasistatic deformation process. The overloaded elements (exceeding a threshold) are removed according to a breaking rule. This corresponds to irreversible microcracking of the lattice. If necessary, a healing mechanism can be implemented as well by restoring the broken elements. The released elastic energy between two successive equilibrium states is fully dissipated by microcracking. The implementation details regarding lattice representation and the resolution of governing equations are described in Appendix A.

In principle, the time step should be small enough in order to have only one critical bond at a time. But this method is hardly feasible, and for a reasonable choice of the time step, several elements may become critical (overloaded) simultaneously. Two possible rules for removing these critical elements are

- only the most critical bond is removed;
- all critical bonds are removed.

A breaking probability as a function of the degree of criticality may also be used (Delaplace et al., 1996; Fitoussi et al., 1998; Herrmann and Roux, 1990; Hu et al., 1998; Van Mier et al., 1997, 2002; Chiaia et al., 1997; Mishnaevsky et al., 2004). In order to optimize the computational effort, we adopt the second solution but with post-relaxation cycles until a equilibrium state is reached before applying the next strain increment. This gives rise to the possibility of crack propagation within one time step. Physically, this corresponds to fast crack propagation compared to deformation rate.

The 2D lattice model has the advantage to be cheap in computational effort, allowing to simulate systems with a large number of nodes for reasonable computing time. The computational effort in solving the set of $2N$ equations by minimizing the potential energy varies in general as N^2. Since in our case N will be huge (as huge as feasible), an important aspect of the algorithm is that its storage requirement should vary only linearly with N. Fortunately in our case, due to the simple additivity of the potential energy, the effort does not grow with N at all. Therefore, the computation time should also depend only linearly on N. The simulations reported in this paper were carried out on samples of at least 4×10^4 nodes. On a 'G5 PowerPC', the CPU time is about 0.01 s per time step and per node.

3. Parameters and notations

We first generate a large dense packing of rigid disk-like particles compressed isotropically by means of the discrete element method. A rectangular portion of this two-dimensional packing is overlaid on a triangular lattice. The starch properties are attributed to the bonds falling inside the particles. The protein is then added in the form of trapezoidal-shape bridges connecting neighboring particles within a prescribed distance (a small fraction of the particle diameter) (Feillet, 2000). The bonds belonging to these bridges are given the properties of the protein matrix. In the same way, the bonds falling between a particle and the matrix or between two particles are given the properties of the corresponding interface. These matrix bridges have variable widths proportional to the total volume of the protein matrix. The samples are bidisperse with particle diameters d_A and $d_B = 0.25d_A$, and with four times more B-type granules. The total particle volume fraction is about 0.80. In the simulations, the protein phase varies from 4% to 20% in volume fraction.

There are three *bulk* phases: (1) particles (starch granules), denoted 'p'; (2) protein matrix, denoted 'm'; and (3) void space or pores, denoted 'v'. There are also two *interface* phases: (1) particle–particle interface, denoted 'pp', and (2) particle–matrix interface, denoted 'pm'. The elements belonging to each phase ϕ (bulk or interface) are given a Hooke constant k^{ϕ} and a breaking force f^{ϕ}. We have $f^v = 0$ and the choice of the value of k^v is immaterial.

In most models of composite materials the interphase 'pp' is neglected, assuming thus that all particles are surrounded by the matrix. In the case of wheat endosperm, however, the particle interactions play a central role and the interface 'pp' should be considered on the same basis as the 'pm' interface. In fact, the surface phases 'pm' and 'pp' are transition zones of finite width. However, the volume fractions of these transition zones can be neglected compared to that of the particles and matrix. The interface phases affect the global behavior through their specific surfaces (total surface per unit volume) and their strengths represented by the Hooke constants k^{pp} and k^{pm} and the corresponding tensile force thresholds f^{pp} and f^{pm}. In our simulations, we model the interface phases by bonds linking two particles or a particle to the matrix. The volume fractions of the interface phases are thus assumed to be zero ($\rho^{pp} = \rho^{pm} = 0$) and the volumes fractions ρ^p, ρ^m and ρ^v are attributed only to the three bulk phases, with

$$\rho^p + \rho^m + \rho^v = 1. \tag{1}$$

It is dimensionally convenient to express the bond characteristics in stress units. We thus define the bond breaking (or debonding) stresses $\sigma^\phi \equiv f^\phi/a$ and the moduli $E^\phi \equiv k^\phi/a$, where a is the length of the lattice vector. These bond moduli E^ϕ of the lattice should be carefully distinguished from the equivalent phase moduli which depend both on the bond moduli and the geometry of the lattice. We will use below square brackets to represent the phase moduli: $E^{[p]}$, $E^{[m]}$, $E^{[pp]}$ and $E^{[pm]}$. For a triangular lattice, stretched orthogonally to a lattice vector, there is a simple relation between the bond stiffness E^ϕ and the equivalent phase stiffness $E^{[\phi]}$ (Schlangen and Garboczi, 1997):

$$E^{[\phi]} = \tfrac{\sqrt{3}}{2} E^\phi. \tag{2}$$

4. Strength properties

We are interested in the influence of two parameters playing a major role in the fracture behavior of the wheat endosperm: the matrix volume fraction ρ^m and the particle–matrix adhesion σ^{pm}. We keep the particle volume fraction constant $\rho^p \simeq 0.8$ and ρ^m is varied from 0.04 to 0.2. At $\rho^m = 0.2$, the whole interstitial space is filled with the protein matrix, corresponding to zero porosity. The behavior in the range $\rho^m < 0.04$ is strongly nonlinear and the initiation and propagation of the cracks strongly depend on the details of the microstructure. The elastic moduli do not seem to be appreciably contrasted among endosperm constituents (Glenn and Johnston, 1992). For this reason, we set $E^p = E^m = E^{pm}$ and $\sigma^p = \sigma^m$. Further parametric study will be necessary to evaluate the effect of local elastic and failure contrasts with respect to the results presented below. The particle–matrix adherence σ^{pm} is varied from $0.3\sigma^{[p]}$ to $1.05\sigma^{[p]}$. We also assume that a fraction of contacts between starch granules are "bare" in the sense that they are not mediated by protein bridges. Since the integrity of the endosperm is supposed to be ensured by the protein matrix, we consider that the bare contacts are cohesionless, i.e. $\sigma^{pp} = 0$.

Each sample contains nearly 400 granules, and each simulation is repeated over three independent configurations. The samples are subjected to uniaxial tension tests by imposing incremental displacement on the upper boundary, see Fig. 2(a). The lower boundary is immobile and the lateral boundaries are free.

Fig. 3 shows the stress–strain plots under tensile loading for three different values of ρ^m and σ^{pm} (belonging to three different regimes of crack propagation, as discussed in Section 5). The corresponding crack patterns are displayed

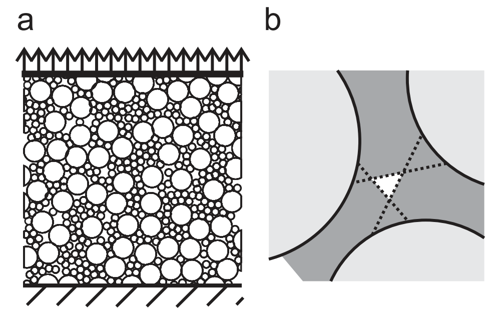

Fig. 2. (a) Boundary conditions of a simple tension test; (b) typical configuration of protein bridges at high protein content, with pores isolated from starch granules.

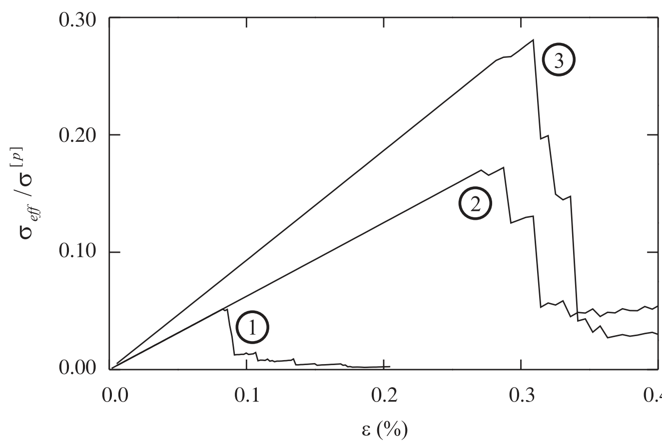

Fig. 3. Stress–strain plots under tensile loading for (1) $\sigma^{pm}/\sigma^{[p]} = 0.6$ and $\rho^m = 0.08$; (2) $\sigma^{pm}/\sigma^{[p]} = 1$ and $\rho^m = 0.08$; and (3) $\sigma^{pm}/\sigma^{[p]} = 1$ and $\rho^m = 0.18$.

in Fig. 4. We observe a brittle behavior with a well-defined initial stiffness E^t_{eff} and a tensile strength σ^t_{eff} defined at the stress peak. The post-peak behavior is characterized by nonlinear propagation of the cracks initiated at the stress peak in the form of a sequence of loading–unloading events. Each event represents the storage of elastic energy followed by energy dissipation as a result of microcracking, i.e. the breaking of one or more bonds. The stiffness declines due to progressive damage of the material. The main crack is perpendicular to the direction of tension. Fig. 4 suggests that the crack path depends more on the protein content than on the starch-granule adherence. This is because the stress inhomogeneities, which are responsible for the stress concentration factor, are more sensitive to the porosity than to adherence among the constituents. It is noteworthy that the observed brittle behavior is a consequence of the local elastic–brittle behavior. The macroscopic behavior can be made more or less ductile or time-dependent by enriching the bond behavior. In the same way, the local strength parameters can be coupled to ambient moisture in order to account for moisture effects at the macroscopic scale (Haddad et al., 2001).

The effective stiffness E^t_{eff} (normalized by $E^{[p]}$) is shown in Fig. 5 as a function of ρ^m for three independent sets of

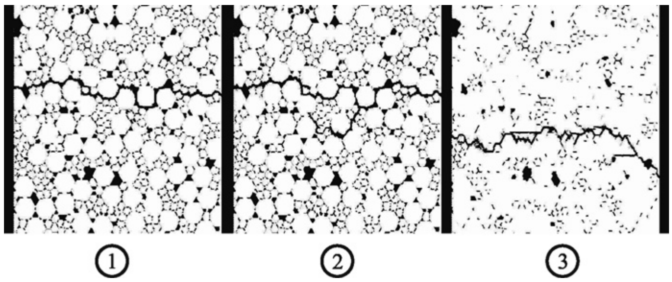

Fig. 4. Crack patterns for (1) $\sigma^{pm}/\sigma^{[p]} = 0.6$ and $\rho^m = 0.08$; (2) $\sigma^{pm}/\sigma^{[p]} = 1$ and $\rho^m = 0.08$; and (3) $\sigma^{pm}/\sigma^{[p]} = 1$ and $\rho^m = 0.18$.

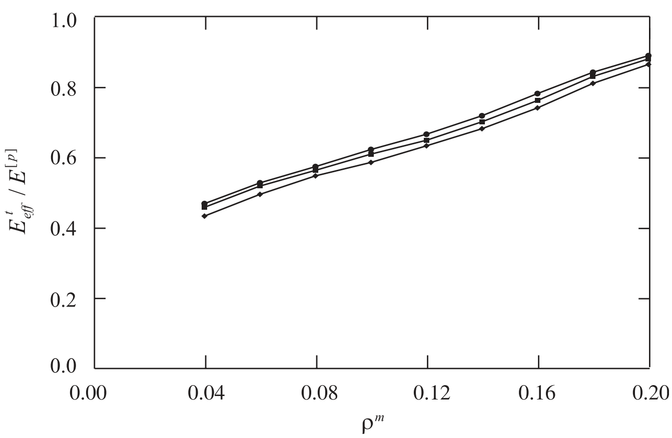

Fig. 5. Effective stiffness E^t_{eff} as a function of the protein volume fraction ρ^m.

configurations. The stiffness E^t_{eff} is nearly linear in ρ^m with a small variability between the three plots. We have $E^t_{eff} < E^{[p]}$ due to porosity and the presence of bare contacts between starch granules (Torquato, 2002). The offset $1 - E^t_{eff}/E^{[p]} \simeq 0.15$ corresponds to the effect of bare contacts in the limit $\rho^m = 1 - \rho^p = 0.2$. The protein matrix has both surface and bulk effects. Hence, the stiffness increases with ρ^m as a result of increasingly homogeneous stress distribution. The surface effect corresponds to the total starch–protein interface which increases with the protein volume fraction and implies growing adherence between the matrix and the particles, as a result.

We approximately have

$$E^t_{eff} = (k_0 + k_1 \rho^m) E^{[p]}, \tag{3}$$

with $k_0 \simeq 0.35$ and $k_1 \simeq 2.5$. This linear increase of stiffness with protein content is consistent with measurements showing larger stiffness in more vitreous wheat grains (Samson et al., 2005).

The tensile strength σ^t_{eff} is a function of both ρ^m and σ^{pm}. Fig. 6 shows a grey-level map of σ^t_{eff} in the parameter space (ρ^m, σ^{pm}). The tensile strength increases smoothly along both axes and the isovalue plots are nearly straight lines. The isovalues show the extent to which the effect of ρ^m for the tensile strength can be replaced by that of σ^{pm}. This means that the endosperm can be very resistant either at

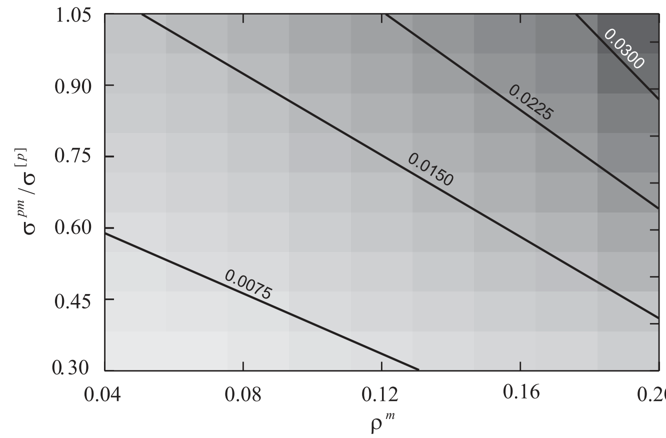

Fig. 6. Grey level map of tensile strength in the parameter space (particle–matrix adherence vs. particle volume fraction).

low protein content with strong adherence between the protein and starch granules or with low adherence and high protein content.

At low ρ^m, the endosperm texture can be qualified as a cohesive granular medium where the protein phase behaves essentially as a binding agent. Increasing ρ^m results in widening of the protein bridge cross section between starch granules and thus enhanced cohesion as would do increasing σ^{pm}. At high ρ^m, the texture can be described as dispersed pores and granules in a continuous protein phase. In this limit, the porosity declines as ρ^m increases, leading to less concentration of stresses and thus enhanced strength and stiffness. The largest value of σ^t_{eff} is $\simeq 0.03\sigma^{[p]}$ and it occurs for $\rho^m = 0.2$ and $\sigma^{pm} = 1.05$. This limit corresponds to strong starch–protein adherence. The low value of σ^t_{eff} in this limit is thus related to the sole effect of bare contacts in tension.

5. Starch damage

In lattice models of fracture, it is common to consider the number of broken elements as a measure of damage (Herrmann and Roux, 1990). Since in wheat grain processing, the fraction of damaged granules is a major signature of the grain hardness (Pomeranz, 1988; Atwell, 2001), we focus here on the proportion n_b of broken elements in the bulk of the granules with respect to the total number of broken elements in the material.

Fig. 7 shows the evolution of n_b as a function of vertical strain for three different sets of parameters. For low enough values of σ^{pm} (plot 1), particle damage is marginal whatever the matrix volume fraction ρ^m. Obviously, the bonds fail in this case favorably at the particle–matrix interface. For a high enough level of σ^{pm} (plots 2 and 3), the fraction n_b remains negligible up to brittle failure where it increases first rapidly, then decreases slightly during the post-peak period as more bonds fail inside the protein matrix and at the starch–protein interface with respect to the bonds failing inside the granules.

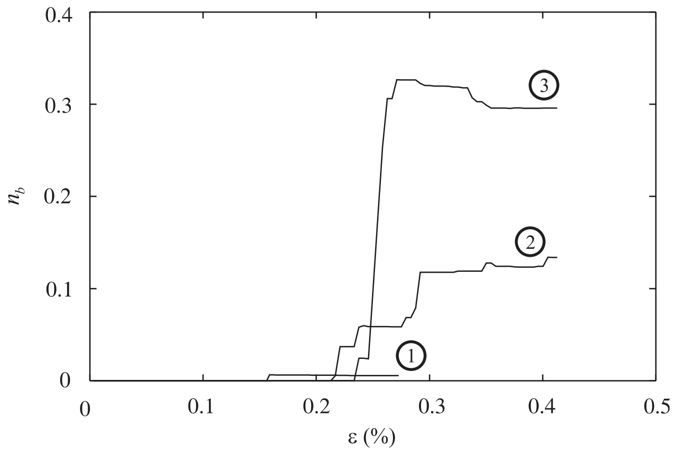

Fig. 7. Evolution of the fraction of broken bonds in the particle phase for (1) $\sigma^{pm}/\sigma^{[p]} = 0.6$ and $\rho^m = 0.08$; (2) $\sigma^{pm}/\sigma^{[p]} = 1$ and $\rho^m = 0.08$; and (3) $\sigma^{pm}/\sigma^{[p]} = 1$ and $\rho^m = 0.18$.

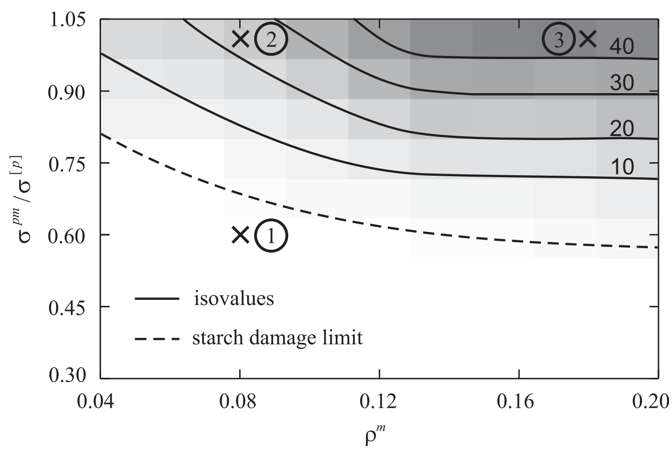

Fig. 8. Grey level map of the fraction of broken bonds inside the starch granules as a function of the protein volume fraction ρ^m and the starch–protein adherence σ^{pm}. Dashed line represents the ''particle damage limit'' as predicted by Eq. (8). The numbers in the circles correspond to the three plots of Figs. 3 and 7.

Fig. 8 shows a map of the fractions n_b in the parameter space. We see that below a well-defined frontier of nearly bilinear shape, no starch damage occurs ($n_b \simeq 0$). For this range of parameters, the cracks propagate in the protein phase and through the pores. Above this ''starch-damage limit'', the isovalue lines are parallel to the limit line with an increasing level of n_b. Remarkably, this line singles out a point corresponding to $\rho^m \simeq 0.12$ and $\sigma^{pm} \simeq 0.6\sigma^p$. For $\rho^m > 0.12$, n_b is independent of ρ^m. The transition at $\rho^m \simeq 0.12$ seems to reflect the percolation of the protein phase throughout the system, with starch granules entirely isolated from the pores by the protein phase; see Fig. 2(b). Beyond this point, increasing the protein content has no consequence for the width of protein bridges between starch granules.

From Fig. 8, we differentiate three regimes of crack propagation: (1) below the starch-damage limit, the cracks bypass starch granules and propagate through the pores

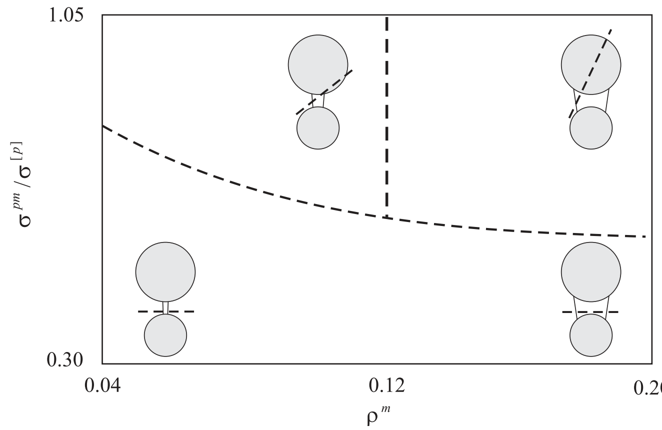

Fig. 9. A schematic representation of cracking regimes.

and the starch–protein interface; (2) above this limit and for $\rho^p < 0.12$, the cracks penetrate also partially into starch granules from protein bridges that strongly concentrate stresses and lead thus to surface abrasion of the granules; (3) above this limit and for $\rho^p > 0.12$, the cracks propagate in the protein phase as well as across the starch granules, causing fragmentation of the granules. These three regimes are schematically represented in Fig. 9.

The starch damage occurs as a result of the penetration of the cracks into the starch granules. According to fracture mechanics, this occurs if the particle is less tough than the matrix–particle interface. Otherwise, the crack will be deflected to the interface (He and Hutchinson, 1989; Buyukozturk and Hearing, 1998). The toughness $K_c = (EG_c)^{1/2}$ of a material combines the stiffness E with the energy G_c required to create a crack of unit surface. In our system, the elastic energy of a matrix–particle bond at failure is $(f^{pm})^2/(2k^{pm})$, and this energy is fully dissipated when the bond fails. Hence, the adhesion energy (per unit length in 2D) is

$$G_c^{pm} = \frac{(f^{pm})^2}{2ak^{pm}}. \tag{4}$$

Using this expression, we define a particle–matrix ''interface toughness'' by

$$K_c^{pm} = (E_{eff}^t G_c^{pm})^{1/2} = \left(\frac{E_{eff}^t}{2E^{pm}}\right)^{1/2} \sigma^{pm}. \tag{5}$$

We also consider the toughness K_c^p of the particles

$$K_c^p = \left(\frac{E^{[p]}}{2E^p}\right)^{1/2} \sigma^p. \tag{6}$$

We substitute the expression of E_{eff}^t as a function of ρ^m from Eq. (3) in (5) and we normalize by K_c^p from Eq. (6) to get the ''relative toughness''

$$K_c^r \equiv \frac{K_c^{pm}}{K_c^p} = (k_0 + k_1\rho^m)^{1/2} \frac{\sigma^{pm}}{\sigma^p}, \tag{7}$$

where we used the fact that $E^{pm} = E^p$ in our simulations.

The important point about the expression of relative toughness K_c^r in Eq. (7) is that it combines explicitly the matrix volume fraction ρ^m with the interphase adherence σ^{pm}. Fig. 10 shows the fraction n_b of broken bonds in the particle phase as a function of σ^{pm}/σ^p for several values of ρ^m. In Fig. 11 we have plotted the same data for all values of ρ^m as a function of K_c^r. It is remarkable that all data points collapse nearly on a single plot with a variability that is essentially of the same order of magnitude as sample-to-sample fluctuations. Below a characteristic toughness $K_c^r \simeq 0.5$, no starch damage occurs. Beyond this point, the fraction of broken bonds increases linearly with K_c^r within the available statistical precision.

The characteristic toughness corresponds physically to transition from a regime where the cracks are deflected to the particle–matrix interface to a regime where the cracks can penetrate into the particles. Eq. (7) enables us to predict the shape of the particle-damage limit in Fig. 8.

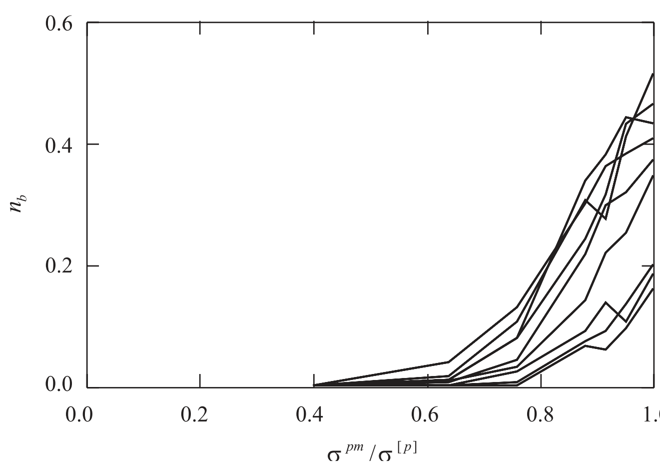

Fig. 10. Fraction of broken bonds inside the starch granules as a function of starch–protein adherence for different values of the protein volume fraction.

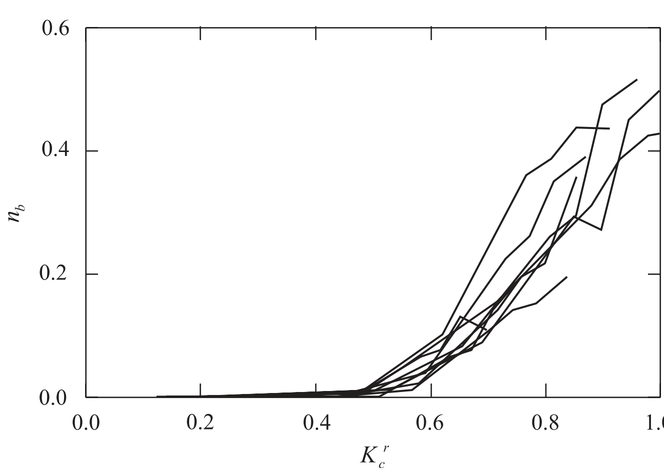

Fig. 11. Fraction of broken bonds inside the starch granules as a function of the relative toughness for different values of the protein volume fraction.

This is the plot of σ^{pm} as a function of ρ^m for $K_c^r \simeq 0.5$. From Eq. (7) we get

$$\sigma^{pm} \simeq 0.5\sigma^p(k_0 + k_1\rho^m)^{-1/2}. \quad (8)$$

This equation is displayed on the grey level map of n_b in Fig. 8 with no other fitting parameters than the values of k_0 and k_1 obtained from Fig. 5. We see that Eq. (8) is a good approximation for the particle-damage limit.

6. Summary and discussion

In this paper, a granular model of the wheat endosperm was introduced and applied to investigate the effect of two major parameters that control the wheat hardness: the protein volume fraction and the starch–protein adherence. This model involves a jammed assembly of starch granules interconnected by the action of the protein matrix. As a result of jamming, the contact zones between the granules are not covered every where by the protein matrix, leading to cleavages or bare contacts that are significant for stress concentration in addition to the effect of the pores. These features make the structure of the wheat endosperm particularly variable, and the mechanical behavior is expected to depend in a complex manner on the filling volume and the nature of the matrix–particle interface. Moreover, the scale-up of interphase adherence to macroscopic stress–strain and yield properties is mediated by the granular structure of the material. Our approach resorts to a lattice-type sub-particle discretization of both the granules and the protein matrix, and incorporates in a simple way the possibility of crack initiation by bond breaking. In order to simulate large representative samples, we opted for efficient algorithms involving simple interactions and rules as well as a quasistatic procedure based on energy minimization.

We studied the stress–strain behavior under simple tension. It was found that the protein volume fraction and the starch–protein adherence play nearly the same role as far as the tensile strength is concerned. But the same parameters control differently the damage characteristics as reflected in the fraction of broken bonds inside starch granules. Indeed, both the interfacial adherence and protein volume fraction are bounded. The adherence is bounded by the internal cohesion of the granules whereas the surface effect of the protein matrix saturates as soon as the protein bridges between the granules percolate. Beyond either of these limits, the particle damage is more sensitive to the starch–protein adhesion than the protein volume fraction.

In particular, there is a starch-damage limit in the parameter space below which no starch damage occurs. In this regime, the cracks propagate either in the protein matrix or at the starch–protein interface. Above the starch-damage limit and below a particular value of the protein volume fraction, corresponding to the percolation threshold of the protein matrix throughout the system, the cracks penetrate also partially into the particles whereas above this particular value of the protein volume fraction, the cracks propagate across the granules causing the fragmentation of starch granules.

Our data suggest that the starch-damage limit is controlled by a single parameter combining the protein volume fraction with the starch–protein adhesion. We showed that this parameter, which scales quite well our starch damage data, corresponds to the relative toughness of the starch–protein interface with respect to the starch toughness. This finding is consistent with the fracture mechanics energetic arguments implying that the penetration of a crack into a particle occurs only if the particle is less tough than the matrix–particle interface. Hence, putting together our main parameters, the relative toughness provides a simple link between starch damage and these parameters.

These findings are of interest to the interpretation of the characterization methods of wheat grains based on post-process analyzes such as the size distribution of the fragments or the starch damage. They elucidate the specific roles of the protein volume fraction and the starch–protein adherence often advocated to explain the hardness of the wheat endosperm. Combining both parameters, the relative toughness links in a simple way the starch damage to these parameters. This is vital information in view of material processing and it provides a quantitative basis for the use of starch damage as a descriptor of wheat hardness.

Our representation of endosperm as an elastic–brittle material in this paper was motivated by the choice of a minimalist system for a detailed parametric study of strength and fracture properties. This model can, however, be greatly enriched in order to incorporate more complex material behaviors for starch and protein materials. In particular, visco-plastic behavior and moisture-dependence properties of the wheat endosperm can be taken into account within this framework. For example, plastic or viscous dissipation could affect our results concerning the relation between starch damage and the interface toughness. Hence, our results can be applied mainly to the case of weak moisture content at high loading rates, as in a dry grinding process.

The results analyzed in this paper were obtained by the application of a unique protocol for the preparation of numerical samples. We varied the phase volume fractions and the adhesion between the phases but the protocol itself did not change. This protocol ensured a nearly homogeneous filling of the interstitial space between the granules, and the bare contacts between touching granules were assumed to be cohesionless. The robustness of our results with respect to the protocol and the influence of the filling procedure require further investigation. In the same way, the influence of the stiffness contrast between starch granules and the protein matrix was not considered in this paper, but it merits a systematic investigation in view of comparison with the effect of the two parameters considered in this paper.

Appendix A. Implementation details

A.1. Lattice representation

We consider a triangular lattice with a rectangular contour. Two types of *geometrical* disorder can be introduced: (1) metric disorder by moving randomly each node to a new position within a given distance. The connectivity (six bonds per node) of the lattice is conserved; (2) topological disorder by removing randomly a fraction of bonds down to the percolation threshold of the lattice. Various types of *material* disorder can be introduced as well into the model. In particular, the elastic properties of the bonds or their thresholds may be attributed according to a prescribed spatial distribution. The latter involves a length scale which in many statistical models of disorder is simply taken to be the mesh length. In our system, this length is given by the average size of the particles, and the properties are uniform in each phase. Hence, if no other geometrical or material disorder is introduced, the lattice is characterized by a *granular disorder* at a mesoscopic scale (as compared to the mesh length); see Fig. 1(b). The stress field is mainly dictated by granular disorder.

In the following, we assume an unstressed triangular lattice with equilibrium bond length a. Usually, a regular lattice is described in terms of multiples (k, l) of its lattice vectors as depicted in Fig. 12(a). This is not very suitable for its management within a computer simulation. A more convenient way is a scheme along the lines of a "stretched checkerboard" as displayed in Fig. 12(b). If there are N_y rows with N_x nodes in an even row and $N_x - 1$ nodes in an odd row, there are N nodes in the system given by

$$N \equiv N_x N_y - N_y/2, \tag{A.1}$$

and its dimensions are (L_x, L_y) given by

$$L_x = N_x a,$$
$$L_y = \sqrt{3}/2 N_y a. \tag{A.2}$$

Notice that all the N nodes can be enumerated in a canonic way according to the following mapping:

$$i = \frac{k + l(2N_x - 1)}{2}. \tag{A.3}$$

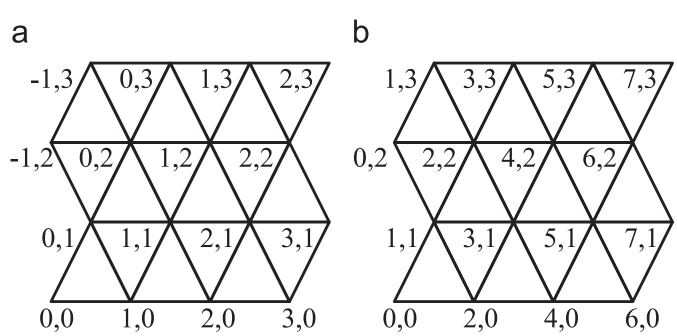

Fig. 12. Two methods for indexing a triangular lattice.

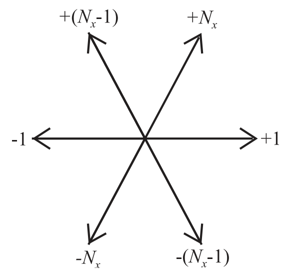

Fig. 13. Indexation of neighboring nodes.

Then, all the neighbors of a node i along the three lattice directions are simply given as in Fig. 13.

A.2. Degrees of freedom

The degrees of freedom of the system are the displacements $\boldsymbol{r}^{k,l}$ of the nodes from the initial positions $\boldsymbol{R}^{k,l}$. We work with the relative displacements

$$\boldsymbol{\Delta}^{k,l} = \boldsymbol{r}^{k,l} - \boldsymbol{R}^{k,l}, \tag{A.4}$$

allowing for larger precision by avoiding to subtract large numbers. Setting $a = 1$, we define the square distances

$$\begin{aligned} 1 + q_0^{k,l} &\equiv (\boldsymbol{r}^{k+2,l} - \boldsymbol{r}^{k,l})^2 \\ &= (\Delta_x^{k+2,l} - \Delta_x^{k,l} + 1)^2 + (\Delta_y^{k+2,l} - \Delta_y^{k,l})^2, \end{aligned} \tag{A.5}$$

$$\begin{aligned} 1 + q_1^{k,l} &\equiv (\boldsymbol{r}^{k+1,l+1} - \boldsymbol{r}^{k,l})^2 \\ &= (\Delta_x^{k+1,l+1} - \Delta_x^{k,l} + 1/2)^2 \\ &\quad + (\Delta_y^{k+1,l+1} - \Delta_y^{k,l} + \sqrt{3}/2)^2, \end{aligned} \tag{A.6}$$

$$\begin{aligned} 1 + q_2^{k,l} &\equiv (\boldsymbol{r}^{k-1,l+1} - \boldsymbol{r}^{k,l})^2 \\ &= (\Delta_x^{k-1,l+1} - \Delta_x^{k,l} - 1/2)^2 \\ &\quad + (\Delta_y^{k-1,l+1} - \Delta_y^{k,l} + \sqrt{3}/2)^2, \end{aligned} \tag{A.7}$$

with $\Delta_x^{k,l} \equiv \boldsymbol{\Delta}^{k,l}.\boldsymbol{e}_x$ and $\Delta_y^{k,l} \equiv \boldsymbol{\Delta}^{k,l}.\boldsymbol{e}_y$. In fact, $\sqrt{1 + q_j^{k,l}}$ is the Euclidean distance between node (k, l) and its neighbors j. In the reference triangular lattice, the values $j = 0, 1, 2$ correspond to the directions along $\boldsymbol{e}_x$,$\boldsymbol{e}_{\pi/3}$ and $\boldsymbol{e}_{2\pi/3}$, respectively.

Setting

$$\begin{aligned} X_0^{k,l} &\equiv \Delta_x^{k+2,l} - \Delta_x^{k,l}, \\ Y_0^{k,l} &\equiv \Delta_y^{k+2,l} - \Delta_y^{k,l}, \end{aligned} \tag{A.8}$$

$$\begin{aligned} X_1^{k,l} &\equiv \tfrac{1}{2}(\Delta_x^{k+1,l+1} - \Delta_x^{k,l}), \\ Y_1^{k,l} &\equiv \tfrac{\sqrt{3}}{2}(\Delta_y^{k+1,l+1} - \Delta_y^{k,l}), \end{aligned} \tag{A.9}$$

$$\begin{aligned} X_2^{k,l} &\equiv -\tfrac{1}{2}(\Delta_x^{k-1,l+1} - \Delta_x^{k,l}), \\ Y_2^{k,l} &\equiv \tfrac{\sqrt{3}}{2}(\Delta_y^{k-1,l+1} - \Delta_y^{k,l}), \end{aligned} \tag{A.10}$$

and temporarily suppressing the indices k, l for the sake of readability, we end up with

$$\begin{aligned} q_0 &= X_0^2 + Y_0^2 + 2.X_0, \\ q_1 &= X_1^2 + Y_1^2 + X_1 + \sqrt{3}Y_1, \\ q_2 &= X_2^2 + Y_2^2 - X_1 + \sqrt{3}Y_1. \end{aligned} \tag{A.11}$$

A.3. Evolution

Each element is characterized by a stiffness and a breaking force threshold. The quantity $(\sqrt{1 + q_j} - 1)$ represents the strain, and the potential energy $U_j^{k,l}$ of a spring of stiffness $E_j^{k,l}$ is expressed as

$$\begin{aligned} U_j &= \frac{E_j}{2}\left(\sqrt{1 + q_j} - 1\right)^2 \\ &= E_j\left(1 + \frac{q_j}{2} - \sqrt{1 + q_j}\right) \\ &= \frac{E_j}{8}\left(q_j^2 - \frac{1}{2}q_j^3\right) + O(q_j^4). \end{aligned} \tag{A.12}$$

This expansion is useful to avoid the computationally costly evaluation of square roots. In this context, a standard procedure would be to substitute the q_j in Eqs. (A.11) into (A.12) in order to obtain a systematic expansion in powers of deformation X_j and Y_j.

In the simulations reported in this paper, an upward (tension) or downward (compression) displacement is imposed on the row $l = N_y$, while at the columns $k = 0$ and $k = 2N_x - 2$ we have open boundary conditions. Imposing stepwise displacement at the boundary and looking for a new equilibrium state at each step corresponds to a quasistatic loading as long as the imposed displacement rate is small compared to the sound speed in the material, which is fulfilled for most practical purposes. Hence, any velocity-dependent behavior of the material must be related only to the breaking rules as discussed below.

The new equilibrium state is determined by minimizing the total potential energy

$$\Psi = \sum_{j,k,l} U_j^{k,l}, \tag{A.13}$$

with respect to the displacements $\boldsymbol{\Delta}^{k,l}$. The conjugate gradient method according to Polak and Ribiere is employed (Press et al., 1996). The key idea behind this algorithm, which needs the gradient of the minimizing function as well, is that the directions in the $2N$-dimensional space of the degrees of freedom, along which line-minimization is performed, are not consecutively perpendicular to each other (as in the straightforward but less efficient steepest descent method) but conjugate in the sense that minimization along a new direction does not spoil the work done for previous directions.

References

Atwell, W., 2001. Wheat Flour. AACC, St Paul, USA.

Barlow, K., Buttrose, M., Simmonds, D., Vesk, M., 1973. The nature of the starch–protein interface in wheat endosperm. Cereal Chemistry 50, 443–454.

Buyukozturk, O., Hearing, B., 1998. Crack propagation in concrete composites influenced by interface fracture parameters. International Journal of Solids and Structures 35, 4055–4066.

Chang, C., Wang, T., Sluys, L., Mier, J.V., 2002a. Fracture modeling using a micro-structural mechanics approach—ii. Finite element analysis. Engineering Fracture Mechanics 69, 1959–1976.

Chang, C.S., Wang, T.K., Sluys, L.J., Mier, J.V., 2002b. Fracture modeling using a micro-structural mechanics approach—i. Theory and formulation. Engineering Fracture Mechanics 69, 1941–1958.

Chiaia, B., Vervuurt, A., Van Mier, J.G.M., 1997. Lattice model evaluation of progressive failure in disordered particle composites. Engineering Fracture Mechanics 57, 301–309.

Cundall, P.A., Strack, O.D.L., 1979. A discrete numerical model for granular assemblies. Géotechnique 29, 47–65.

Delaplace, A., Pijaudier-Cabot, G., Roux, S., 1996. Progressive damage in discrete models and consequences on continuum modelling. Journal of the Mechanics and Physics of Solids 44, 99–136.

Delenne, J.Y., 2002. Granular media with solid behaviour—modelling, experimental analysis of the cohesion, validation and applications. Ph.D. Thesis, Université Montpellier II.

Dobraszczyk, B.J., 1994. Fracture mechanics of vitreous and mealy wheat endosperm. Journal of Cereal Science 19, 273–282.

Feillet, P., 2000. Le grain de blé: composition et utilisation. INRA, Paris.

Feng, S., Thorpe, M.F., Garboczi, E., 1985. Effective-medium theory of percolation on central-force elastic networks. Physical Review B 31, 276–280.

Fitoussi, J., Guo, G., Baptiste, D., 1998. A statistical micromechanical model of anisotropic damage for s.m.c. composites. Composites Science and Technology 58, 759–763.

Gao, H., Klein, P., 1998. Numerical simulation of crack growth in an isotropic solid with randomized internal cohesive bonds. Journal of the Mechanics and Physics of Solids 46, 187–218.

Glenn, G., Johnston, R., 1992. Mechanical properties of starch, protein and endosperm and their relationship to hardness in wheat. Food Structure 11, 187–199.

Greenwell, P., Schofield, J.D., 1986. A starch granule protein associated with endosperm softness in wheat. Journal of Cereal Science 63, 379–380.

Haddad, Y., Benet, J.C., Delenne, J.Y., Mermet, A., Abecassis, J., 2001. Rheological behaviour of wheat endosperm—proposal for classification based on the rheological characteristics of endosperm test samples. Journal of Cereal Science 34, 105–113.

He, M.-Y., Hutchinson, J.W., 1989. Crack deflection at an interface between dissimilar elastic materials. International Journal of Solids and Structures 25, 1053–1067.

Herrmann, H.J., Roux, S., 1990. Statistical Models for Fracture in Disordered Media. North-Holland, Amsterdam.

Hu, G.K., Guo, G., Baptiste, D., 1998. A micromechanical model of influence of particle fracture and particle cluster on mechanical properties of metal matrix composites. Computational Materials Science 9, 420–430.

Lilliu, G., Van Mier, J.G.M., 2003. 3D lattice type fracture model for concrete. Engineering Fracture Mechanics 70, 927–941.

Mishnaevsky Jr., L., Derrien, K., Baptiste, D., 2004. Effect of microstructure of particle reinforced composites on the damage evolution: probabilistic and numerical analysis. Composites Science and Technology 64, 1805–1818.

Moreau, J.J., 1994. Some numerical methods in multibody dynamics: application to granular materials. European Journal of Mechanics A/Solids (Supp. 4), 93–114.

Morris, C., 2002. Puroindolines: the molecular genetic basis of wheat grain hardness. Plant Molecular Biology 48, 633–647.

Piot, O., Autran, J.C., Manfait, M., 2000. Spatial distribution of protein and phenolic constituents in wheat grain as probed by confocal Raman microspectroscopy. Journal of Cereal Science 32, 57–71.

Pomeranz, Y., 1988. Wheat: Chemistry and Technology. AACC, St Paul, USA.

Prado, E.P., van Mier, J.G.M., 2003. Effect of particle structure on mode I fracture process in concrete. Engineering Fracture Mechanics 70, 1793–1807.

Press, W.H., Flannery, B., Teukolsky, S.A., Vetterling, W.T., 1996. Numerical Recipes in Fortran 90: The Art of Parallel Scientific Computing, Fortran Numerical Recipes, vol. 2. Cambridge University Press, Cambridge.

Radjaï, F., Preechawuttipong, I., Peyroux, R., 2000–2001. Cohesive granular texture. In: Vermeer, P.A., Diebels, S., Ehlers, W., Herrmann, H.J., Luding, S., Ramm, E. (Eds.), Continuous and Discontinuous Modelling of Cohesive-Frictional Materials, Lecture Notes in Physics, vol. 568, Springer, Berlin/ Heidelberg, p. 149.

Roux, S., 1990. Continuum and discrete description of elasticity and other rheological behavior. In: Herrmann, H.J., Roux, S. (Eds.), Statistical Models for Fracture in Disordered Media. Elsevier, North Holland, Amsterdam, pp. 87–114.

Samson, M., Mabille, F., Chéret, R., Abécassis, J., Morel, M., 2005. Mechanical and physicochemical characterization of vitreous and mealy durum wheat endosperm. Cereal Chemistry 82, 81–87.

Schlangen, E., Garboczi, E.J., 1997. Fracture simulations of concrete using lattice models: computational aspects. Engineering Fracture Mechanics 57, 319–332.

Torquato, S., 2002. Random Heterogeneous Materials—Microstructure and Macroscopic Properties. Springer, New York.

Turnbull, K.M., Rahman, S., 2002. Endosperm texture in wheat. Journal of Cereal Science 36, 327–337.

Van Mier, G.M.J., Chiaia, M.B., Vervuurt, A., 1997. Numerical simulation of chaotic and self-organizing damage in brittle disordered materials. Computer Methods in Applied Mechanics and Engineering 142, 189–201.

Van Mier, J.G.M., Van Vliet, M.R.A., 1999. Experimentation, numerical simulation and the role of engineering judgement in the fracture mechanics of concrete and concrete structures. Construction and Building Materials 13, 3–14.

Van Mier, J.G.M., van Vliet, M.R.A., Wang, T.K., 2002. Fracture mechanisms in particle composites: statistical aspects in lattice type analysis. Mechanics of Materials 34, 705–724.

Vogel, H.-J., Hoffmann, H., Leopold, A., Roth, K., 2005a. Studies of crack dynamics in clay soil: II. A physically based model for crack formation. Geoderma 125, 213–223.

Vogel, H.-J., Hoffmann, H., Roth, K., 2005b. Studies of crack dynamics in clay soil: I. Experimental methods, results, and morphological quantification. Geoderma 125, 203–211.